Mechanism underlying impaired cardiac pacemaking rhythm during ischemia: A simulation study

Xiangyun Bai, Kuanquan Wang, Yongfeng Yuan, Qince Li, Halina Dobrzynski, Mark R. Boyett, Jules C. Hancox, and Henggui Zhang

Citation: Chaos **27**, 093934 (2017);
View online: https://doi.org/10.1063/1.5002664
View Table of Contents: http://aip.scitation.org/toc/cha/27/9
Published by the American Institute of Physics

Mechanism underlying impaired cardiac pacemaking rhythm during ischemia: A simulation study

Xiangyun Bai,[1,2] Kuanquan Wang,[1] Yongfeng Yuan,[1] Qince Li,[1] Halina Dobrzynski,[3] Mark R. Boyett,[3] Jules C. Hancox,[2,4] and Henggui Zhang[1,2,5,a)]
[1]*School of Computer Science and Technology, Harbin Institute of Technology, Harbin 150001, China*
[2]*Biological Physics Group, School of Physics and Astronomy, The University of Manchester, M13 9PL Manchester, United Kingdom*
[3]*Institute of Cardiovascular Sciences, The University of Manchester, M13 9PL Manchester, United Kingdom*
[4]*Department of Physiology and Cardiovascular Research, School of Medical Sciences, The University of Bristol, Bristol BS8 1TD, United Kingdom*
[5]*Space Institute of Southern China, Shenzhen, China*

(Received 9 March 2017; accepted 31 August 2017; published online 20 September 2017)

Ischemia in the heart impairs function of the cardiac pacemaker, the sinoatrial node (SAN). However, the ionic mechanisms underlying the ischemia-induced dysfunction of the SAN remain elusive. In order to investigate the ionic mechanisms by which ischemia causes SAN dysfunction, action potential models of rabbit SAN and atrial cells were modified to incorporate extant experimental data of ischemia-induced changes to membrane ion channels and intracellular ion homeostasis. The cell models were incorporated into an anatomically detailed 2D model of the intact SAN-atrium. Using the multi-scale models, the functional impact of ischemia-induced electrical alterations on cardiac pacemaking action potentials (APs) and their conduction was investigated. The effects of vagal tone activity on the regulation of cardiac pacemaker activity in control and ischemic conditions were also investigated. The simulation results showed that at the cellular level ischemia slowed the SAN pacemaking rate, which was mainly attributable to the altered Na^{+}-Ca^{2+} exchange current and the ATP-sensitive potassium current. In the 2D SAN-atrium tissue model, ischemia slowed down both the pacemaking rate and the conduction velocity of APs into the surrounding atrial tissue. Simulated vagal nerve activity, including the actions of acetylcholine in the model, amplified the effects of ischemia, leading to possible SAN arrest and/or conduction exit block, which are major features of the sick sinus syndrome. In conclusion, this study provides novel insights into understanding the mechanisms by which ischemia alters SAN function, identifying specific conductances as contributors to bradycardia and conduction block.

[http://dx.doi.org/10.1063/1.5002664]

Sinus bradycardia, a phenotype of sick sinus syndrome (SSS), may be caused by sinoatrial node (SAN) ischemia. Recent experimental studies have focused on characterizing ischemia-induced changes to membrane ion channels of nodal cells. However, it is still unclear how such changes at the cellular ion channel level may cause sinus bradycardia, compromising the ability of the SAN to pace and drive the surrounding atrium, given that the cardiac pacemaker is an integrative and complex nonlinear system. In this study, we address these issues with multi-scale models of the SAN, from single cell to 2D SAN-atrium tissue levels. The functional impact of ischemia-induced electrophysiological changes on cardiac pacemaking action potentials and their conduction was investigated. Effects of vagal tone activity on the regulation of cardiac pacemaker activity in control and ischemic conditions were also studied. The results provide new insights into understanding the mechanism by which ischemia causes cardiac pacemaker dysfunction, and why SSS patients have significantly lower heart rates (even sudden death) at night when the vagal tone is high.

I. INTRODUCTION

The sinoatrial node (SAN), the pacemaker of the mammalian heart, possesses intrinsic automaticity. Dysfunction of the SAN may lead to abnormal cardiac rhythms, manifested by intermittent sinus bradycardia, sinus arrest, sinus pause, slow SAN-atrium conduction, sinus exit block or alternating bradycardia and atrial tachycardia.[1,2]

SAN dysfunction may arise from a variety of conditions, such as ageing,[3] gene mutations,[4,5] and cardiac ischemia.[6] In the latter case, the sinus node artery, which carries the main blood supply to the SAN, may suffer from hypoperfusion, causing ischemia that impairs SAN function. Experimental studies have shown that occlusion of the sinus node artery produces various dysrhythmias, including sinus slowing and

a)Author to whom correspondence should be addressed: henggui.zhang@manchester.ac.uk

sinoatrial block.[7–9] With decreasing sinus rhythm, cardiac output and blood pressure decreases, and in some extreme cases, sinus arrest may occur causing sudden death.[10] Although ischemia-induced SAN dysfunction can be fatal, the exact underlying ionic mechanisms remain elusive.

Prior studies have been carried out to characterize the effects of ischemia on the electrophysiological properties of mammalian atrial and ventricular myocytes (e.g., Refs. 11–13). It has been found that ischemia is associated with acidosis, hyperkalemia and hypoxia, each of which produces alterations to the electrophysiological properties of cardiac cell and tissues, including changes to ion channel properties and intercellular electrical coupling.[12,14] These changes may be responsible for the genesis of cardiac arrhythmias during ischemia.[14,15] However, there is little experimental information on the effects of ischemia on the electrophysiological properties of SAN due to its complicated and heterogeneous anatomy. Experimental evidence suggests that ischemia can also modulate ion channel function in SAN cells, producing an increased L-type calcium channel current (I_{CaL})[16] and hyperpolarization activated inward current (I_f), but decreased T-type calcium channel current (I_{CaT}), rapid and slow components of the rectifier potassium channel currents (I_{Kr} and I_{Ks}), and Na^+-Ca^{2+} exchanger activity (I_{NaCa}).[6,16,17] However, it is still unclear if the changes identified at the cellular ion channel level are sufficient to account for the ischemia-induced sinus bradycardia, a nonlinear behaviour arising from the interactions of millions of SAN cells. The relative roles of ischemia-induced changes to altered particular ion channel currents in compromising SAN pacemaking activity and the ability of the SAN to drive the surrounding atrial muscle are yet to be elucidated. Acetylcholine (ACh), the neurotransmitter released by the vagal nerves is known to slow down the pacemaking rate (PR).[18–20] Measurements from anaesthetized dogs have demonstrated that vagal action on the heart rate can be potentiated during SAN ischemia.[21] However, whether and how the vagal activity compromises the SAN pacemaking activity during ischemia has not yet been elucidated.

Computational models of the heart have provided powerful tools to study the functional effects of gene mutations,[4,5] heart failure,[22,23] and ageing[24,25] on cardiac pacemaker activities. Being constructed from, and validated against experimental data, they provide a means for quantitatively predicting the functional roles of altered molecular dynamics and ionic channels in a systematic way that is difficult to achieve in an experimental setting.[4,26,27] In previous computational work, Butters *et al.* showed that *SCN5A* gene mutations are causally linked to the sick sinus syndrome.[4] Modelling has also been used to investigate the mechanisms by which ankyrin-B defects increase susceptibility to SAN dysfunction and atrial fibrillation and the functional impact of heart failure on SAN.[28,29] In this study, we developed multi-scale (cell and tissue) models of the rabbit SAN-atrium in control and ischemic conditions. Using these models we investigated the functional impact of ischemia on the initiation and conduction of SAN action potentials and their conduction into the atrium.

II. METHODS

A. Mathematical models of single cell and 2D SAN-atrium tissue

The consequences of ischemia-induced electrophysiological alterations for SAN cells were investigated by using: (1) electrophysiologically detailed central and peripheral SAN cell models;[30] (2) a 2D anatomical model of the intact SAN-atrium tissue, incorporating accurate single cell models of the SAN[30] and the right atrium (RA),[31] together with the reconstructed tissue geometry.[32] These single cell models have been validated in prior studies.[30,31] In numerical simulations, the time step was chosen to be 0.01 ms at the cellular level. In the 2D intact SAN-atrium model, we used the same time step with a space step of 0.04 mm which gave accurate numerical solutions.

B. 2D tissue slice model

The 2D anatomical model of the intact SAN-atrium tissue used in this study was reconstructed from histological and immunohistochemistry imaging data.[32] In brief, the model considered distinct regions of the SAN-atrium, with consideration of the intrinsic electrical heterogeneity in the atria and central and peripheral SAN cells.[32,33] The anatomical geometry of the model was based on the reconstructed endocardial surface of the 3D SAN-atrium tissue[32] (see Fig. S1 in the supplementary material), which was discretized by a high spatial resolution of 0.04 mm to form a regular Cartesian grid of 385×250 nodes. Each node had a flag variable to identify the cell type (the SAN central, peripheral and RA cell), based on immunohistochemistry mapping data.[32] The central and peripheral SAN cells were modelled by the Zhang *et al.* equations,[30] and atrial cells of the RA were modelled by the Aslanidi *et al.* equations.[31]

Similar to our prior studies,[4,34] in the 2D intact SAN-atrial tissue model we incorporated local variations of cellular electrophysiology as observed experimentally; these included regional differences of cell membrane capacitance (C_m), the diffusion coefficient (D; as a determinant of conduction velocity) and cellular electrophysiological properties[32] (see Fig. S2 in the supplementary material). Spatial distributions of current densities were correlated with the cell membrane capacitance, C_m, which increases gradually from the centre to the periphery of the SAN.[30,34] The gradient distribution of D was introduced according to Zhang *et al.*[34] In order to model the effects of ACh on SAN cells, the ACh-activated K^+ current, $I_{K,ACh}$ was incorporated, I_{CaL} was partially inhibited, and the activation curve of I_f was shifted toward more negative potentials. Detailed equations and parameters used in the model have been given in the work of Butters *et al.*[4] The 2D anatomical model of the intact SAN-atrium was validated by its ability to reproduce the correct sequence of action potential (AP) initiation and conduction through the rabbit intact SAN-atrium, as found experimentally[3,35] (see Fig. S1in the supplementary material).

TABLE I. Ischemia-induced electrophysiological changes in rabbit SAN cells. All the experimental data on ischemia-induced ion channel remodeling were from rabbit SAN cells with 5 or 7 min ischemia. Other experimental data were based on rabbit ventricular cells with mild ischemia condition.

Changed factors	Percentage of change (normalized to control condition)	Changed factors	Percentage of change (normalized to control condition)
g_{CaL}	↑110% (Ref. 16)	g_{Na}	↓25% (Refs. 14 and 37)
g_{CaT}	↓36.8% (Ref. 6)	$[Na^+]_i$	↑66% (Refs. 49 and 50)
g_{Kr}	↓16% (Ref. 6)	ATP_i (mmol/l)	4.6 (Refs. 38 and 45)
g_{Ks}	↓26% (Ref. 6)	ADP_i (μmol/l)	99 (Refs. 38 and 45)
k_{NaCa}	↓42% (Ref. 6)		
g_f ($g_{f,Na}$ and $g_{f,K}$)	↑15.3% (Ref. 16)	$[K^+]_o$	↑50% (Refs. 38 and 39)

C. Ischemic SAN model

1. Changes to ion channel currents

In order to model effects of ischemia on the SAN, the conductances of some of the main ionic channel currents responsible for cellular depolarization and repolarization were adjusted, based on experimental data on the effects of ischemia on the rabbit SAN (see Table I).[6,16] These changes include an increased L-type calcium channel conductance (g_{CaL}; increased by 110%),[16] a decreased T-type calcium channel conductance (g_{CaT}; decreased by 36.8%),[6] decreased rapid- and slow-delayed rectifier potassium channel conductance (g_{Kr} and g_{Ks}; decreased by 16% and 26% respectively)[6] and decreased Na^+/Ca^{2+} exchanger (g_{NaCa}; decreased by 42%)[6] current. It was shown in a previous experimental study that in "ischemic" Tyrode's solution the funny current (I_f) of SAN cells increased by 15.3% at −60 mV.[16] As sodium channel current (I_{Na}) is present in the peripheral SAN cells and does contribute to the pacemaking and driving ability of the SAN,[30,36] an ischemia-induced reduction in the channel conductance (g_{Na}; decreased by 25%)[14,37] as observed in ventricular cells was also considered in simulations (see Table I, the right column).

2. Hyperkalemia

For simulating hyperkalemia during ischemia, the extracellular potassium concentration ($[K^+]_o$) was elevated by 50% as observed experimentally.[38,39]

3. ATP-sensitive channel current (I_{KATP}) due to hypoxia

Previous experimental studies suggest that the metabolic depletion-activated K-ATP channel current (I_{KATP}) may play an important role in the pathogenesis of SAN dysfunction during cardiac ischemia.[40,41] It has been shown that I_{KATP} channel openers regulate the maximum diastolic potential (MDP) and pacemaking rates of rabbit SAN cells.[42,43] Similar functional effects of I_{KATP} on regulation of cardiac pacemaking APs have also been observed in mice during hypoxia.[41,44] Therefore, in simulations we incorporated the I_{KATP} formulation developed by Ferrero *et al.*[45] Details of the I_{KATP} formulation can be found in the supplementary material.

4. Changes of ionic homeostasis and energy metabolism

The homeostasis of H^+ in rabbit SAN cells is maintained by the Na^+/H^+ exchanger,[46] which may lead to an increased intracellular Na^+ concentration ($[Na^+]_i$) during ischemia. In addition, some other studies from ventricular cells have found that the intracellular free Na^+ concentration is increased due to the hypoxia-induced depletion of the cellular ATP content.[47,48] However, these experimental data are absent for rabbit SAN cells. In order to consider all possible actions of ischemia in simulations, some data from ventricular ischemia experiments were also considered, including changes in intracellular ATP (ATP_i), the extracellular ADP (ADP_i), and the intracellular Na^+ concentration. For details, please see Table I.

III. RESULTS

A. SAN effects of ischemia at the single cell level

The effects of ischemia-induced changes on cellular ion channels and ion homeostasis (see Table I) on spontaneous action potentials of SAN cells were first investigated. The results are shown in Fig. 1, in which simulated action

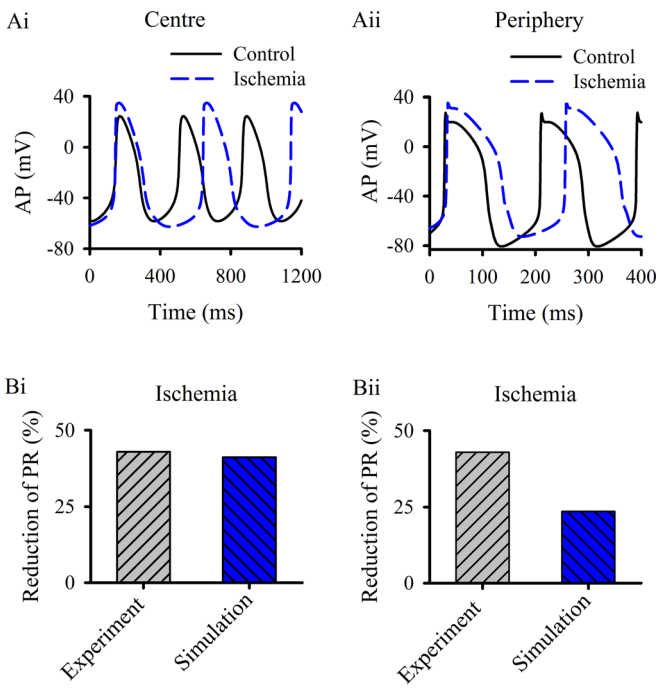

FIG. 1. Effects of ischemia on SAN action potentials. (a) Simulated action potentials in control and ischemic conditions for central (ai) and peripheral (aii) cells. (b) Effects of ischemia on the pacemaking rate (PR) of central (bi) and peripheral (bii) cells. Simulation data were compared with the experimental data of Du and Nathan.[6]

potentials in the ischemic condition are superimposed on those in the control condition [Fig. 1(a)]. Ischemia increased the overshoot of the APs, which corresponded to the experimental observation of Du and Nathan;[6] prolonged the action potential duration, and hyperpolarized the MDP in the central cell model, but depolarized the MDP in the peripheral cell model. In both cell models, the phase-4 depolarisation process was slowed down, leading an increased pacemaking cycle length (PCL; the time interval between two successive pacemaking APs); consequently there was a deceleration of the pacemaking rate. Ischemia increased PCL by about 41.2% in the central cell model, which was close to the experimental data of Du and Nathan[6] (PCL increased by 43%). A 23.5% increase of PCL in the peripheral cell model was observed, which was somewhat smaller than experimental data[6] [as shown in Fig. 1(b)]. Therefore, our simulation results show that the ischemia-induced changes in ion channel currents, ionic concentrations, and the activation of I_{KATP} are sufficient to account for the bradycardia observed in ischemic rabbit SAN cells. The more depolarised MDP in the peripheral cell model with ischemia matched the experimental observation of Du and Nathan.[6] The modest hyperpolarization of MDP in the central cell model with ischemia differed from the experimental data of Du and Nathan.[6] In the study of Du and Nathan,[6] SAN cells were isolated from a rectangular piece of nodal tissue with a size of (1.0–1.5) $\times$ (3.0–3.5) mm located at about 0.5–1.0 mm from the crista terminalis (CT), with cell capacitance ranging from 20 pF to 62 pF; this wide range of cell sizes suggests that the isolated cell population may have contained both central (small capacitance) and peripheral (large capacitance) cells. In simulations, our cell models considered the intrinsic regional heterogeneity of the SAN,[31] which assumed a cell capacitance of 20 pF for the central cell and 65 pF for the peripheral cell models. This may account for the discrepancy between the simulation and the experimental data of Du and Nathan for the modest hyperpolarized membrane potential.

The roles of each individual ischemia-induced cellular change in alterations to SAN cell APs were investigated by using either an "inclusive" method or an "exclusive" method. With the inclusive method, each individual ischemic action was considered alone in simulations. With the exclusive method, the individual ischemic action of interest was excluded from the integral action of ischemia. Figure 2 shows the results obtained from the inclusive method. It illustrates that in both the central and peripheral cell models the ischemia-induced increase of I_{CaL} played a primary role in prolonging the action potential duration (APD) (by 20.0% in the central cell [Fig. 2(ai); and by 26.9% in the peripheral cell model], whilst the elevation of $[Na^+]_i$ abbreviated APD (by 24.0% in the central cell model and by 2.3% in the peripheral cell model). Other ischemic actions on ionic channel currents, ion concentration or the activation of I_{KATP} had non-marked effects with respect to APD prolongation.

In the central cell model, the ischemia-induced decreases of I_{CaT} and I_{NaCa}, the activation of I_{KATP} and the increase of $[Na^+]_i$ contributed markedly to the slowing down of the pacemaking APs, producing an increased cycle length (PCL) [Fig. 2(bi)] (by 6.1%, 3.9%, 11.1% and 84.8% respectively). The

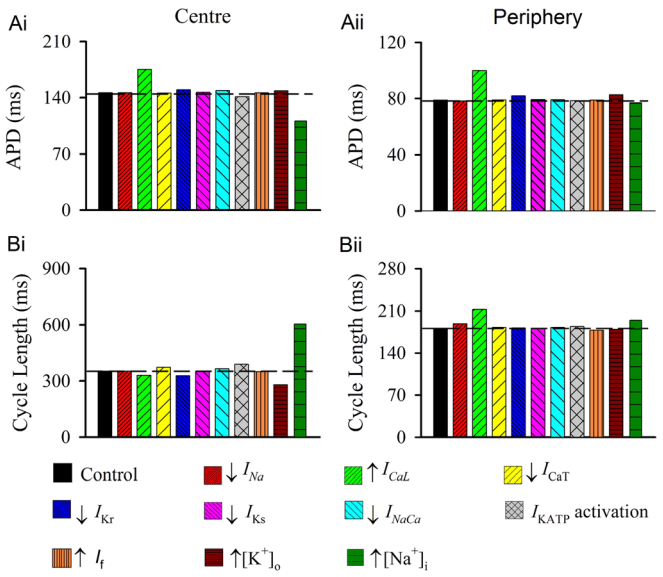

FIG. 2. Role of each individual ischemic action on APD (a) and pacemaking cycle length (b) for central (ai) and (bi) and peripheral (aii) and (bii) cells. APD was measured at a membrane potential of −30 mV.

increased I_f reduced PCL (by 0.86%) in the central cell model. Note that in the central cell model, the increase in $[Na^+]_i$ during SAN ischemia produced the largest increase in PCL. For the peripheral cell model, results were different from those in the central cell model due to their intrinsic differences in ion channel properties.[21,25] Our results suggested that the altered I_{CaT}, I_{Kr}, I_{Ks}, and I_{NaCa} had almost no effect on PCL in the peripheral cell model [Fig. 2(bii)], while the ischemia-induced decrease of I_{Na}, activation of I_{KATP}, increases of $[Na^+]_i$ and I_{CaL} caused an increase of PCL by 3.9%, 1.4%, 7.2%, and 17.2%, respectively. Note that in the peripheral cell model the increase of I_{CaL} contributed the most to the PCL increase, which resulted from an increase of the APD as shown in Fig. 2(aii). Simulations from the exclusive method showed similar results with respect to the influence of each individual ischemic action on SAN APs to the inclusive method, as shown in Figs. S3, S4, and S5 in the supplementary material.

Further simulations were performed to elucidate the mechanisms by which the $[Na^+]_i$ increase ($[Na^+]_i = 13.28$ mM) during ischemia slowed down pacemaking. The results are shown in Fig. 3 for central (left panels) and peripheral (right panels) cells in control and $[Na^+]_i$. In both cell models, it was found that an increased $[Na^+]_i$ resulted in an increased PCL and more hyperpolarized MDP [Figs. 3(ai) and 3(aii)]. It reduced the AP amplitude and duration in the center model, but not in the periphery model. These changes in AP profiles were associated with an increased I_{NaK} [Figs. 3(ci) and 3(cii)], a reversed operating mode of I_{NaCa} (i.e., increased the outward component) [Figs. 3(di) and 3(dii)], all of which contributed to the slowing down of the pacemaking rate, though there was an increased I_f [Fig. 3(ei)] due to a more hyperpolarized MDP. In simulation, an increased $[Na^+]_i$ had more a prominent effect in the central cell model than in the periphery cell model, which was attributable to the differences in ion channel properties of the two cell types.[21,25]

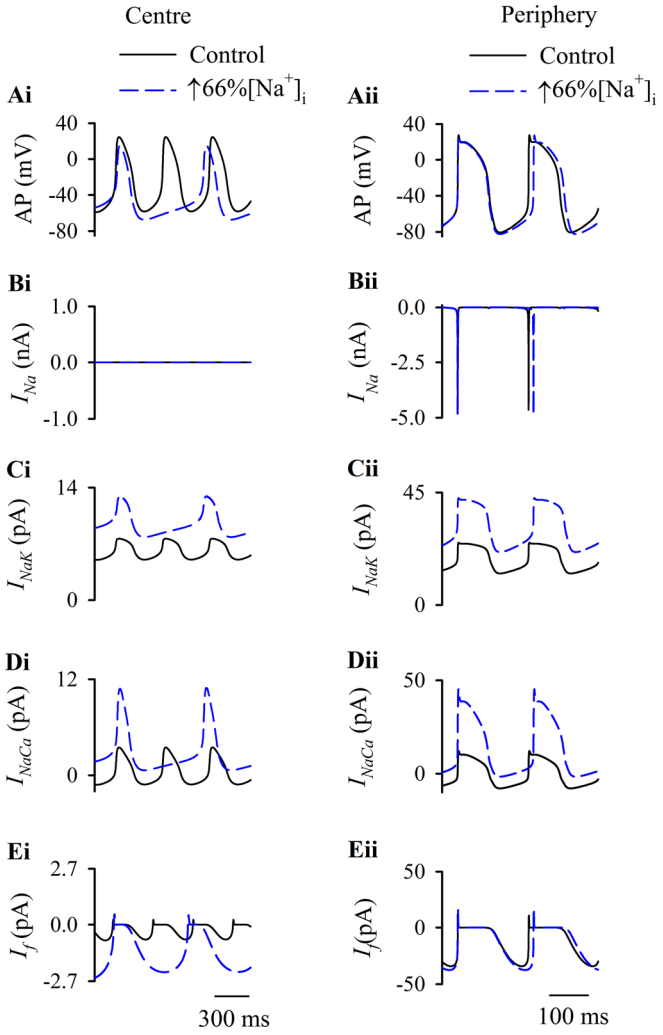

FIG. 3. Effects of intracellular sodium overload on spontaneous action potentials and underlying ion currents for central [left panels, (ai)–(ei)] and peripheral [right panels, (aii)–(eii)] SAN cells. (a) action potentials. (b) I_{Na}. (c) I_{NaK}. (d) I_{NaCa}. (e) I_f.

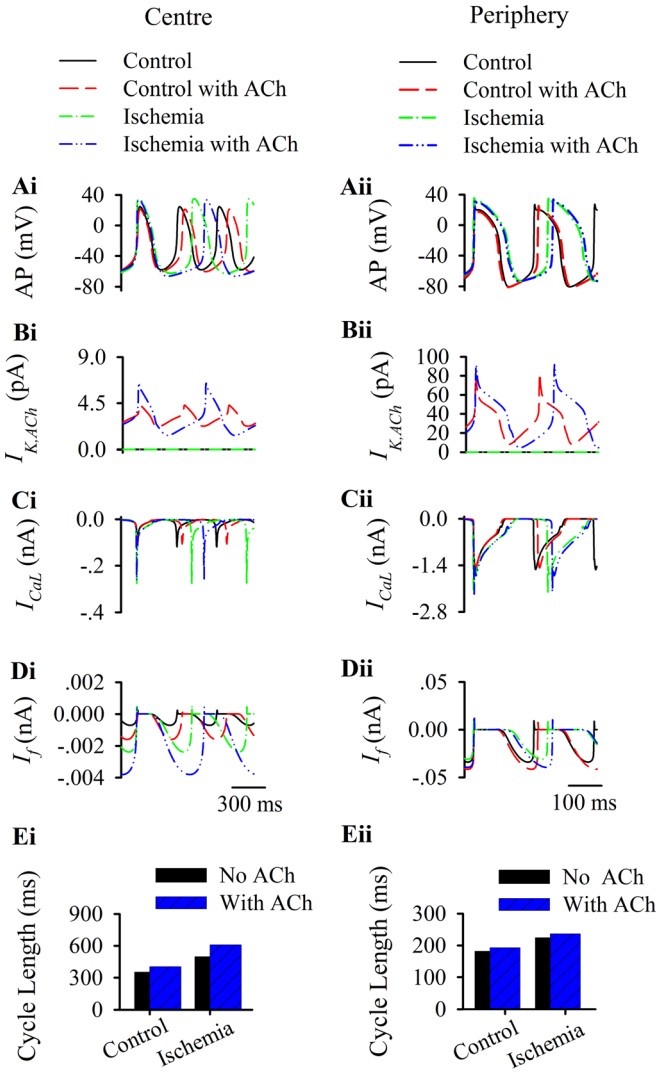

FIG. 4. Effects of ACh under control and ischemic conditions. Simulated action potentials and underlying currents of the central (ai)–(di) and peripheral (aii)–(dii) SAN cells. [ACh] $= 3.0 \times 10^{-8}$ mol/l. (a) APs; (b) $I_{K,ACh}$; (c) $I_{Ca,L}$; (d) I_f; (e) Pacemaking cycle length in central (ei) and peripheral (eii) cells.

B. Effects of ACh on SAN cell activity

ACh has been established to slow down pacemaking by increasing the PCL in both central and peripheral SAN cells, with a larger effect on the central cells.[38,45] It is not known whether the negative chronotropic action of ischemia is augmented by ACh. To address this question, further simulations were performed in which effects of ACh on SAN APs in control and ischemic conditions were studied. The results are shown in Fig. 4. In the control condition, the simulated effects of a "physiological" ACh concentration ([ACh] $= 3.0 \times 10^{-8}$ mol/l) [18–20] resulted in the PCL increasing from 352.5 ms to 403.2 ms (by 14.4%) for the central cell [Fig. 4(ai)], and from 181.4 ms to 192.7 ms (by 6.2%) for the peripheral cell [Fig. 4(aii)]. The negative chronotropic effect of ACh was due to the integrated actions of activation of $I_{K,ACh}$ [Fig. 4(b)], changes in $I_{Ca,L}$ [Fig. 4(c)] and I_f [Fig. 4(d)]. In the ischemic condition, application of ACh increased the PCL of the central and peripheral cell models by 72.9% and 30.2% respectively compared to control; these changes were markedly greater than those under ischemic condition (i.e., PCLs were increased by 41.2% and 23.5% respectively as compared to control condition). As such, the negative chronotropic effects of ACh were amplified by ischemia in both the centre and the peripheral cell models.

The dose-dependent effects of ACh on APs in control and ischemic conditions were also considered. Figure 5 presents the results obtained from the central and peripheral cell models for various "physiological" [ACh].[18–20] It shows that an increase of ACh concentration resulted in an increase in the PCL of both cell types. The negative chronotropic effect of all ACh concentrations was amplified by ischemia. At an ACh concentration of 8.0×10^{-8} mol/l, central SAN cells still exhibited pacemaking (though with a prolonged PCL) in the control condition, but became quiescent in the ischemic condition [Fig. 5(bi)]. Similar results were seen in the ischemic peripheral cell at an ACh concentration of 4.0×10^{-7} mol/l [Fig. 5(cii)]. Figure 5(d) summarizes the simulated dose-dependent effect of ACh on PCLs in control and ischemic conditions. It shows that ischemia shifted the dose-dependence of the PCL leftwards, indicating a more suppressive effect of ACh on SAN cells during ischemia.

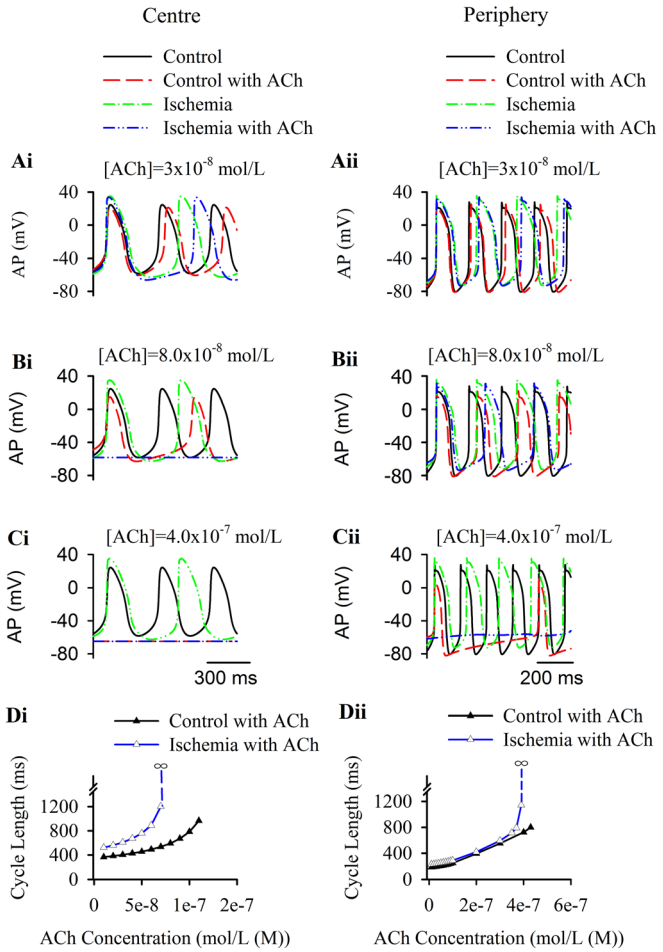

FIG. 5. Dose-dependent effect of ACh on central [left panels, (ai)–(di)] and peripheral [right panels, (aii)–(dii) SAN cells. (a)–(c), effects of varying ACh concentrations on APs. (d) Dose-dependence of PCL.

C. Two-dimensional tissue effects

Due to the electrotonic interaction between the SAN and atrium, the functional impact of ischemia seen at the isolated single-cell level may be different to that seen in the intact SAN-atrium tissue level. Thus, in addition to single cell simulations, multicellular tissue models must be used to evaluate the functional consequences of ischemia and ACh in the setting of ischemia. Therefore, simulations of activity from intact SAN-atrium tissue under control and ischemia conditions were conducted, the results of which are shown in Fig. 6.

Figure 6(ai) shows the snapshots of the initiation and conduction pattern of pacemaking APs in the 2D SAN-atrium model under control condition at different timings. The AP was first initiated in the centre of the SAN. Once initiated, the AP propagated preferentially from the centre towards the periphery of the SAN, and then to the crista terminalis (CT) before entering the atrium in the direction towards the right atrium. However, in the direction towards the atrial septum, the AP conduction was blocked in the conduction block zone, which was encircled by excitation waves from the superior and inferior tissues surrounding the zone. The simulated activation and AP conduction pattern in the 2D model matches prior experimental data from the rabbit heart.[31]

Figure 6(aii) plots the spatial (running vertically) and temporal (running horizontally) profiles of APs [recorded from representative cells along the black line across the SAN-atrium model as shown in Fig. 6(ai)] for three consecutive cycles, demonstrating a stable excitation and conduction pattern in the intact SAN-atrium model. The measured PCL was about 367 ms, which is close to experimental data obtained from multicellular tissue recordings of the intact SAN-atrium of the rabbit heart.[31] Note that the measured PCL at the tissue level was greater than that of isolated central SAN cells, which controlled the pacemaking rhythm of the SAN. This is due to the electrotonic interaction between the SAN and the atrium,[31] which depressed the pacemaking APs of SAN cells as observed experimentally in previous studies.[31,51]

SAN ischemia [Fig. 6(bii)] or application of ACh (1.0×10^{-6} mol/l) [Fig. 6(cii)] in the 2D model did not alter AP conduction patterns (the relative snapshots of the initiation and conduction pattern of the pacemaking action potentials in the 2D tissue shown in Figs. 6(bi) and 6(ci) but shifted the leading pacemaking sites towards the periphery by 0.12 mm in both conditions. An ACh-induced shift in the leading pacemaker site has been observed experimentally by optical mapping.[52] In simulations, SAN ischemia and ACh also slowed down pacemaking rate, resulting in a PCL of 396 and 560 ms, respectively. It is of interest that AP conduction was also slowed, as demonstrated by the slower spread of the excitation wavefront in the tissue, as compared to control tissue shown in Fig. 6(ai). In the normal tissue, the excitation wavefront spread over the 2D tissue model by about 80 ms, which increased to 90 and 120 ms in SAN ischemia and ACh conditions, respectively.

Combined actions of ACh (1.0×10^{-6} mol/l) and ischemia amplified the negative chronotropic effects of each intervention. The results are shown in Fig. 6(di) for the activation pattern and 6(dii) for the space-time plots of APs from the representative cells in the tissue. With an integrated action of both ACh and SAN ischemia, SAN pacemaking activity was further slowed, with a measured PCL of 593 ms. It is also notable that the original leading pacemaking site was shifted toward the periphery SAN, and a region in the peripheral SAN tissue close to the superior vena cava became a secondary leading pacemaking site. The APs generated by either site were unable to drive the surrounding atrial muscle, leading to conduction exit block-a phenomenon typically seen in the sick sinus syndrome. With an increased ACh concentration during ischemia, SAN exit block became more likely to occur than in the control condition with the same level of ACh (data are not shown).

Detailed analyses were also performed to investigate the mechanisms by which ischemia affects APs and conduction in the intact SAN-atrial tissue model and PCL. The results are shown in Fig. 7. Figure 7(a) plots the measured activation time for the representative cells across the tissue in control, ischemia and in ACh with and without ischemia; the corresponding conduction velocity of APs across the tissue was calculated and shown in Fig. 7(b). Both ischemia and ACh increased the activation *time, but* the latter had greater effects, indicating an increased time required for the AP to

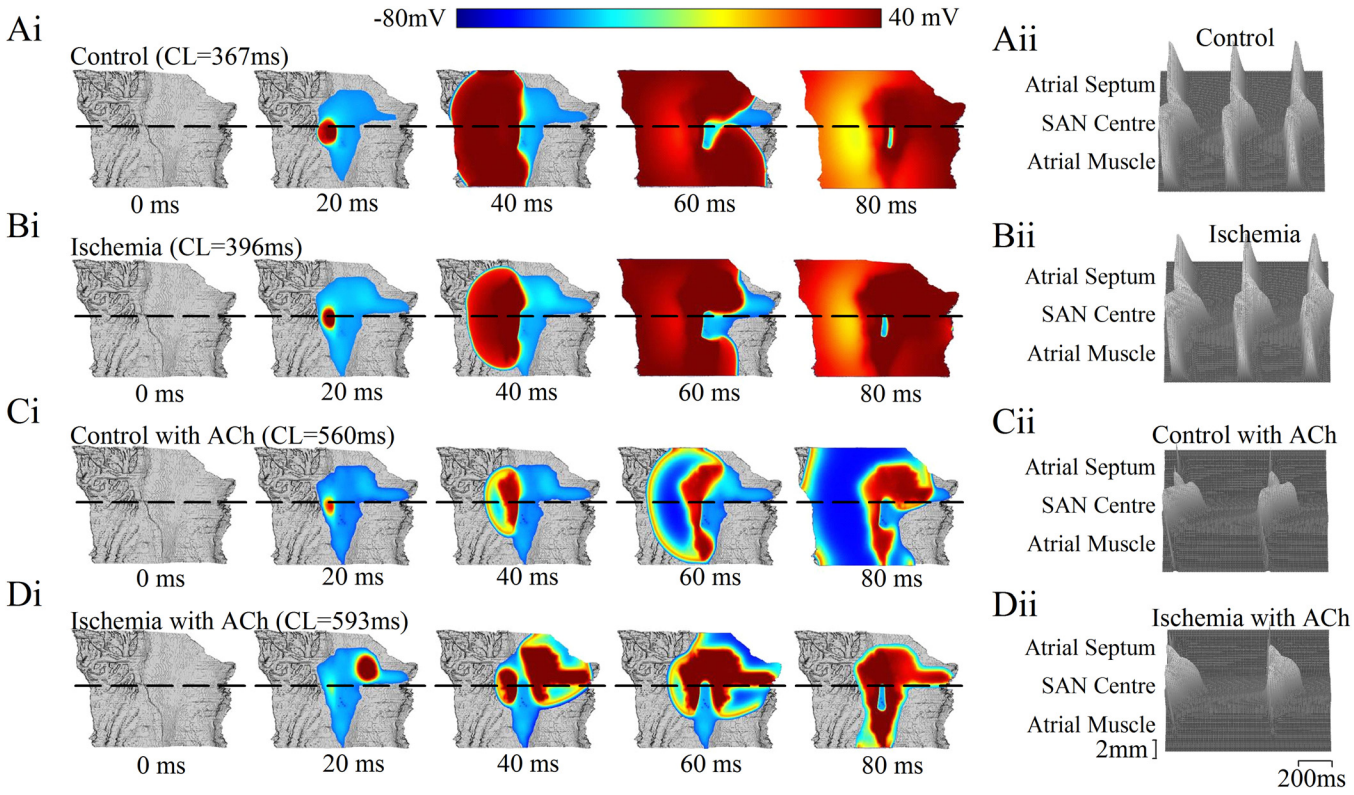

FIG. 6. ACh effect on AP initiation and conduction in the 2D intact SAN-atrial tissue. [ACh] $= 1.0 \times 10^{-6}$ mol/l. (Ai) – (Di) the snapshots of the initiation and conduction pattern of pacemaking APs in the 2D SAN-atrium. Each snapshot mapped with different colours, which changed from blue for −80 mV to red for 40 mV. (Aii) – (Dii) The spatial (running vertically) and temporal (running horizontally) profiles of APs (recorded from representative cells along the black dash line across the SAN-atrium model as shown in figure (Ai) – (Di) for three consecutive cycles.

conduct from SAN to the atrial muscle. In Fig. 7(a), the sinoatrial-atrium activation time was reduced in the direction towards the atrium septum in the ischemia and ACh condition [blue line in Fig. 7(a)]. This was due to the presence of two leading pacemaking sites in that condition, one of which was at the peripheral region of the SAN that was close to the right atrium (i.e., the leading pacemaker site shifted, see Fig. 6(di), snapshot at 40 ms), therefore, the time taken to reach the right atrium was decreased, though the sinoatrial-atrium conduction was actually slowed down. The increased activation time in the direction towards the crista terminalis corresponded to a decreased AP conduction velocity as shown in Fig. 7(b). The increased activation time and the corresponding decreased conduction velocity were attributable to a decreased upstroke velocity of cellular APs as shown in Fig. 7(c). Ischemia reduced dV/dt_{max} in both right atrium and SAN, with a greater effect on the right atrium. Application of ACh further reduced dV/dt_{max} in ischemic tissue, most severely in the SAN peripheral region. A decreased dV/dt_{max} in both SAN peripheral regions indicated a reduced driving power of the SAN and an increased electrical load of the atrium to the SAN, resulting in an increased PCL and even a SAN conduction exit block, in which case the SAN failed to drive the atrial muscle.

IV. DISCUSSION

In this study, we modeled the electrophysiological activities of central and peripherial SAN cells during ischemia based on experimental data, and incorporated these models into an electrophysiologically and anatomically detailed 2D intact rabbit SAN-atrium model. We investigated the functional role of ischemia-induced alterations at the cellular level to elucidate which and how these may cause SAN bradycardia during ischemia, and whether or not these alterations play the same functional role in both central and peripheral SAN cells. With the tissue model, we further investigated the functional effects of SAN ischemia in impairing the ability of the SAN to pace and drive the surrounding atrial muscle. Our simulation results provide evidence substantiating the causative link between SAN ischemia and sinus bradycardia. The major findings of this study are as follows: (1) at the cellular level, the ischemia-induced bradycardia in both central and peripheral cells can be attributed to the intracellular Na^+ increase, I_{KATP} activation, increased I_{CaL}, and the reverse mode of I_{NaCa}; (2) at the intact SAN-atrium tissue level, ischemia decreased the pacemaking rate and slowed down the AP conduction across the SAN-atrium; (3) the bradycardiac effects of SAN ischemia are likely to be amplified by vagal nerve activity: simulated addition of ACh to the tissue with ischemia not only slowed pacemaking and AP conduction, but also compromised the ability of the SAN to pace and drive the atrium, leading to a higher probability of conduction block at the SAN-atrium junction (a phenomenon known as SAN exit block); this effect was greater than that seen with ACh alone. This finding may provide further insight into the mechanism underlying high risk of cardiac arrest in ischemic patients at night, when the vagal tone is greater.[47,53]

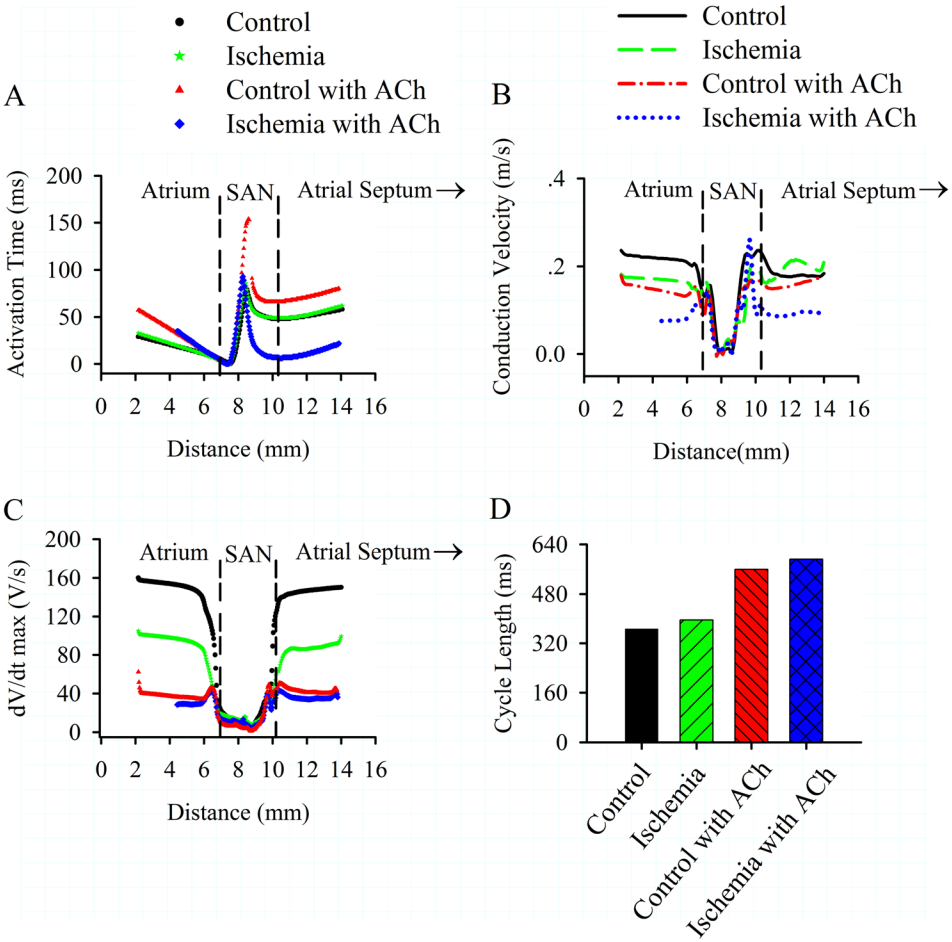

FIG. 7. The effect of ACh on AP conduction in the normal (Control) tissue and 2D tissue with SAN ischemia. (A) Activation times with ischemia and ACh compared with control condition; (B) and (C) the relative conduction velocity and dV/dt_{max}; (D) PCL in the 2D tissue in the different simulated conditions, showing augmented effects when ischemia is combined with ACh ($[ACh] = 1.0 \times 10^{-6}$ mol/l).

A. Ischemia and impaired pacemaking activity

At the cellular level, the main causes of bradycardia with simulated ischemia are $[Na^+]_i$ overload and I_{KATP} activation in central SAN cells, and an increased I_{CaL} (mainly prolonged APD, slowing down the repolarization phase) (Fig. 2, Bi and Fig. S4 in the supplementary material). Previous experiments on rabbit SAN cells have demonstrated that the MDP changed and pacemaking rate slowed with the addition of ATP-sensitive K^+ channel openers.[42,43] Our simulated effect of I_{KATP} is concordant with these experimental findings. Experimental data have shown that Na^+-K^+ pump activity was increasingly inhibited during ventricular ischemia leading to intracellular Na^+ overload.[54] We assumed that a similar intracellular $[Na^+]_i$ overload may also occur during SAN ischemia. The combined effect of the augmented reverse-mode of I_{NaCa} and/or I_{NaK}, and intracellular Na^+ overload further slowed down pacemaking significantly. However, in the peripheral cell model the causative link between SAN ischemia and bradycardia is not exactly the same as in the central cell model. In the peripheral cell model, the increased I_{CaL} and intracellular $[Na^+]_i$ are the major causes of bradycardia, while I_{KATP} activation has little effect. The rise in intracellular $[Na^+]_i$ resulted in functional changes in ion channel currents (Fig. 3) similar to those in the central cell. Altogether, our simulation results suggest that ischemia-induced changes in I_{NaCa} and I_{CaL}, and activation of I_{KATP} play important roles in ischemia-induced bradycardia, which could be potential targets for the treatment of SAN effects of ischemia. Reduction of I_{CaT} had little effect on AP in our simulation results (Fig. 2) as some prior experimental/modelling studies found.[55–57]

At the intact SAN-atrium tissue level, ischemia slowed down the pacemaking rate, as well as the AP conduction (AP) (Fig. 6). The simulation results of slowed AP conduction through the SAN-atrium during ischemia are in agreement with experimental observations.[58]

We simulated the effect of ischemia by considering both ischemia-induced changes to various ionic currents by altering their maximum membrane conductances and altered $[K^+]_o$ and $[Na^+]_i$. As altered $[K^+]_o$ and $[Na^+]_i$ might produce a secondary effect on the membrane ion channel currents of interest, further simulations were conducted to dissect such a combined process. For this, six different scenarios were considered, and the results are shown in the Fig. S6 (in the supplementary material). The six cases are:

(i) Combined effects of all altered ion channel conductances (including a decreased conductance of I_{Kr}, g_{Kr}) and elevated $[K]_o$ and $[Na^+]_i$ [full ischemia condition considered; results are shown in Figs. S6(ai) and S6(aii), supplementary material for central and peripheral cell models, respectively];

(ii) Altered all other ion channel currents with elevated $[K]_o$ and $[Na^+]_i$, but without reduction in g_{Kr} [results are shown in Figs. S6(bi) and S6(bii), supplementary material];

(iii) Like (i), but with a smaller decrease in g_{Kr} [results are shown in Fig. S6(ci), S6(cii); S6(di), S6(dii), supplementary material].
(iv) Like (i), but without elevated $[K]_o$ [results are shown in Figs. S6(ei) and S6(eii), supplementary material for central and peripheral cell models respectively];
(v) Like (i), but without elevated $[Na^+]_i$ [results are shown in Figs. S6(fi) and S6(fii), supplementary material];
(vi) Altered ion channel conductances only but without elevated $[K]_o$ and $[Na^+]_i$ [results are shown in Figs. S6(gi) and S6(gii), supplementary material].

For all cases, the computed reduction in the pacemaking rate is presented in Figs. S6(hi) and S6(hii), supplementary material.

As compared to case (i), in the presence of elevated $[K^+]_o$, without reducing g_{Kr} [Figs. S6(bi) and S6(bii), supplementary material] or with a smaller g_{Kr} reduction [Figs. S6(ci) and S6(cii) and S6(di) and S6(dii), supplementary material], the simulated results were comparable to the case (i) (i.e., considering both of all affected ion channels and elevated $[K^+]_o$). In case (iv), due to un-elevated $[K^+]_o$, greater potassium channel currents led to an even greater bradycardia effect [Figs. S6(ei) and S6(eii), supplementary material], as manifested by a marked increase in the reduction of pacemaking rate [PR; see Figs. S6(hi) and S6(hii), supplementary material]. Therefore, isolating ischemic effects on ion channel currents from elevated $[K^+]_o$ do not alter the conclusion drawn from Fig. 1.

In the absence of an elevated $[Na^+]_i$ (with normal $[Na^+]_i = 8$ mM, $E_{Na} = 76.45$ mV; with elevated $[Na^+]_i = 13.28$ mM, $E_{Na} = 62.91$ mV), the PR was increased in the central SAN cell model but decreased in the periphery SAN cell model [Figs. S6(fi) and S6(fii), supplementary material]. Further analysis (Fig. S7, supplementary material) illustrated that without an elevated $[Na^+]_i$, I_{NaK} and the outward mode of I_{NaCa} was reduced [Figs. S7(ci) and S7(di), supplementary material], resulting in a depolarized MDP and shortened depolarization phase. Though I_f was decreased [Fig. S7(bi), supplementary material], but more depolarized MDP (MDP ≈ -40 mV) directly activated I_{CaL}, resulting in faster pacemaking APs as compared to the full ischemic condition. In the periphery cell model, un-elevated $[Na^+]_i$ also decreased I_{NaK}, the outward I_{NaCa} and I_{Na} [Figs. S7(cii), S7(dii), and S7(eii), supplementary material], but has little effect on I_f due to the negligible change in MDP. Such a combined effect of these altered four currents slightly increased PR as compared with the ischemia condition (case i) [Fig. S7(aii), supplementary material], but still decreased the PR as compared with the control condition [Fig. S6(hii), supplementary material].

In case (vi), in the absence of elevated $[K^+]_o$ and $[Na^+]_i$, a decreased PR in both center and periphery cell models was observed, which was smaller as compared to that in case (i) [Figs. S6(hi) and S6(hii), supplementary material].

B. ACh effects on the ischemic SAN

Previous studies have confirmed the negative chronotropic effect of ACh on cardiac pacemaking cells.[18–20] However, until now there has been a paucity of information about effects of ACh on ischemic SAN. The present study addresses this issue. With increasing ACh concentrations, a more suppressive effect of ACh on ischemic SAN has been shown at both cellular and 2-D tissue levels. The augmented bradycardiac effect of ACh can be attributed to the reduction of I_f (Fig. 4), as well as the activation of $I_{K,ACh}$.

Our simulations demonstrated synergistic effects of ACh and ischemia: ACh not only further slows down the pacemaking rate in ischemic SAN cells, but also impairs the ability of the SAN to drive the surrounding atrial muscle, as revealed by the results shown in Figs. 6 and 7. It was shown that ACh caused failure of AP conduction from SAN to the atrium in the ischemic condition, which may contribute to the observed conduction failure risks, e.g., atrial fibrillation[59] or sinus arrest[7] (even sudden death) at night when the vagal tone is high.

C. Limitations

The limitations of the rabbit cell and tissue models used in our study have been described previously.[30,31] In order to produce ischemic SAN cell models, we modified the equations for I_{CaL}, I_{CaT}, I_{Kr}, I_{Ks}, I_{NaCa}, and I_f based on available experimental data from rabbit SAN cells.[6,16,17] Other changes incorporated into our models came from mammalian ventricular ischemia experiments.[14,37,38,45,49,50] The I_{KATP} formulation here was based on that from a guinea pig ventricular cell model.[45] In cases where data from a specific species/cell type are unavailable, it is accepted practice to use data from other species or cell-types in cardiac modeling. In this regard, it is notable that our simulation results of ischemia-induced bradycardia at the single-cell level showed good agreement with experimental data from ischemic rabbit SAN cells,[6,16] suggesting that the parameters in our ischemic models are reasonable. Although our 2D anatomical tissue model considered the intrinsic electrical heterogeneity of SAN-atrial tissue, further 3-D anatomical models may be required to investigate fully AP initiation in the SAN and conduction from SAN toward atrium (e.g., to establish precise locations of the sinus exit block sites with different concentrations of ACh and/or with different extents of SAN ischemia), which may depend on the details of the tissue spatial structure, 3D heterogeneity and anisotropy. Nevertheless, although the dimensions of our tissue model have been reduced from full 3-D to 2-D, the results of our simulations provide valuable insights into mechanistic links between SAN ischemia and ischemia-induced sinus bradycardia. Moreover, gap junction uncoupling may happen during SAN ischemia as reported in ventricular ischemia,[60] which warrants further study by using bi-domain models to capture gap junction remodeling during ischemic conditions.

SUPPLEMENTARY MATERIAL

See supplementary material for the model equations, parameters and additional results.

ACKNOWLEDGMENTS

This work was funded by The National Natural Science Foundation of China (61572152 and 61571165), Shenzhen

Science and Technology Innovation Committee (JCYJ20151029173639477; JSGG20160229125049615), EPSRC (UK) (EP/J00958X/1), and BHF (FS/14/15/30533).

[1]P. E. Vardas, E. N. Simantirakis, and E. M. Kanoupakis, Circulation **127**(23), 2343–2350 (2013).
[2]M. I. Ferrer, Circulation **47**(3), 635–641 (1973).
[3]A. M. Alings and L. N. Bouman, Eur. Heart J. **14**(9), 1278–1288 (1993).
[4]T. D. Butters, O. V. Aslanidi, S. Inada, M. R. Boyett, J. C. Hancox, M. Lei, and H. Zhang, Circ. Res. **107**(1), 126–137 (2010).
[5]A. O. Verkerk and R. Wilders, Europace **16**(3), 384–395 (2014).
[6]Y. M. Du and R. D. Nathan, J. Mol. Cell. Cardiol. **42**(2), 315–325 (2007).
[7]M. Kotoku, A. Tamura, S. Naono, and J. Kadota, Heart Vessels **22**(6), 389–392 (2007).
[8]E. H. Cushing, H. S. Feil, E. J. Stanton, and W. B. Wartman, Br. Heart J. **4**(1–2), 17–34 (1942).
[9]G. Ando, A. Gaspardone, and I. Proietti, Heart **89**(2), E5 (2003).
[10]R. M. Robertson, New Engl. J. Med. **343**(17), 1259–1260 (2000).
[11]Q. Zhou, X. Zhou, Z. L. TuEr-Hong, H. Wang, T. Yin, Y. Li, L. Zhang, Y. Lu, Q. Xing, J. Zhang, Y. Yang, and B. Tang, Int. J. Cardiol. **203**, 187–195 (2016).
[12]J. M. Di Diego and C. Antzelevitch, Heart Rhythm **8**(12), 1963–1968 (2011).
[13]C. Dussault, H. Toeg, M. Nathan, Z. J. Wang, J. F. Roux, and E. Secemsky, Circ.: Arrhythmia Electrophysiol. **8**(2), 263–269 (2015).
[14]E. Carmeliet, Physiol. Rev. **79**(3), 917–1017 (1999).
[15]J. M. Ferrero, B. Trenor, and L. Romero, Europace **16**(3), 405–415 (2014).
[16]Y. M. Du and R. D. Nathan, Am. J. Physiol. - Heart Circ. Physiol. **293**(5), H2986–H2994 (2007).
[17]O. Gryshchenko, J. Qu, and R. D. Nathan, Am. J. Physiol. - Heart Circ. Physiol. **282**(6), H2284–H2295 (2002).
[18]D. DiFrancesco and C. Tromba, J. Physiol. **405**, 477–491 (1988).
[19]A. Noma and W. Trautwein, Pflugers Arch.: Eur. J. Physiol. **377**(3), 193–200 (1978).
[20]B. Sakmann, A. Noma, and W. Trautwein, Nature **303**(5914), 250–253 (1983).
[21]E. K. Potter, D. I. McCloskey, and G. P. Courtice, Clin. Sci. **71**(4), 449–451 (1986).
[22]J. Constantino, Y. Hu, A. C. Lardo, and N. A. Trayanova, Am. J. Physiol. - Heart Circ. Physiol. **305**(8), H1265–H1273 (2013).
[23]J. F. Gomez, K. Cardona, and B. Trenor, J. Mol. Cell. Cardiol. **89**(Pt B), 146–159 (2015).
[24]R. V. Oren and C. E. Clancy, PLoS Comput. Biol. **6**(12), e1001041 (2010).
[25]V. V. Fedorov, A. V. Glukhov, and R. Chang, Am. J. Physiol. - Heart Circ. Physiol. **302**(9), H1773–H1783 (2012).
[26]S. Inada, H. Zhang, J. O. Tellez, N. Shibata, K. Nakazawa, K. Kamiya, I. Kodama, K. Mitsui, H. Dobrzynski, M. R. Boyett, and H. Honjo, PloS One **9**(4), e94565 (2014).
[27]A. V. Maltsev, Y. Yaniv, M. D. Stern, E. G. Lakatta, and V. A. Maltsev, Circ. Res. **113**(10), e94–e100 (2013).
[28]R. M. Wolf, P. Glynn, S. Hashemi, K. Zarei, C. C. Mitchell, M. E. Anderson, P. J. Mohler, and T. J. Hund, Am. J. Physiol. - Heart Circ. Physiol. **304**(9), H1253–H1266 (2013).
[29]A. O. Verkerk, M. M. van Borren, A. C. van Ginneken, and R. Wilders, Front. Physiol. **6**, 18 (2015).
[30]H. Zhang, A. V. Holden, I. Kodama, H. Honjo, M. Lei, T. Varghese, and M. R. Boyett, Am. J. Physiol. - Heart Circ. Physiol. **279**(1), H397–H421 (2000).
[31]O. V. Aslanidi, M. R. Boyett, H. Dobrzynski, J. Li, and H. Zhang, Biophys. J. **96**(3), 798–817 (2009).
[32]H. Dobrzynski, J. Li, J. Tellez, I. D. Greener, V. P. Nikolski, S. E. Wright, S. H. Parson, S. A. Jones, M. K. Lancaster, M. Yamamoto, H. Honjo, Y. Takagishi, I. Kodama, I. R. Efimov, R. Billeter, and M. R. Boyett, Circulation **111**(7), 846–854 (2005).
[33]W. K. Bleeker, A. J. Mackaay, M. Masson-Pevet, L. N. Bouman, and A. E. Becker, Circ. Res. **46**(1), 11–22 (1980).
[34]H. Zhang, Y. Zhao, M. Lei, H. Dobrzynski, J. H. Liu, A. V. Holden, and M. R. Boyett, Am. J. Physiol. - Heart Circ. Physiol. **292**(1), H165–H174 (2007).
[35]E. E. Verheijck, A. Wessels, A. C. van Ginneken, J. Bourier, M. W. Markman, J. L. Vermeulen, J. M. de Bakker, W. H. Lamers, T. Opthof, and L. N. Bouman, Circulation **97**(16), 1623–1631 (1998).
[36]H. Honjo, M. R. Boyett, I. Kodama, and J. Toyama, J. Physiol. **496**(Pt3), 795 (1996).
[37]Y. Kagiyama, J. L. Hill, and L. S. Gettes, Circ. Res. **51**(5), 614–623 (1982).
[38]N. Venkatesh, J. S. Stuart, S. T. Lamp, L. D. Alexander, and J. N. Weiss, Circ. Res. **71**(6), 1324–1333 (1992).
[39]J. T. Vermeulen, H. L. Tan, H. Rademaker, C. A. Schumacher, P. Loh, T. Opthof, R. Coronel, and M. J. Janse, J. Mol. Cell. Cardiol. **28**(1), 123–131 (1996).
[40]D. B. Shaw, N. J. Linker, P. A. Heaver, and R. Evans, Br. Heart J. **58**(6), 598–607 (1987).
[41]K. Fukuzaki, T. Sato, T. Miki, S. Seino, and H. Nakaya, J. Physiol. **586**(11), 2767–2778 (2008).
[42]X. Han, P. E. Light, W. R. Giles, and R. J. French, J. Physiol. **490**(Pt 2), 337–350 (1996).
[43]H. Satoh, J. Cardiovasc. Pharmacol. **22**(6), 863–868 (1993).
[44]A. V. Glukhov, T. P. Flagg, V. V. Fedorov, I. R. Efimov, and C. G. Nichols, J. Mol. Cell. Cardiol. **48**(1), 152–160 (2010).
[45]J. M. Ferrero, Jr., J. Saiz, J. M. Ferrero, and N. V. Thakor, Circ. Res. **79**(2), 208–221 (1996).
[46]D. Kikeri and M. L. Zeidel, J. Am. Soc. Nephrol. **1**(6), 890–901 (1990).
[47]W. Baust, B. Bohnert, and O. Riemann, Electroencephalogr. Clin. Neurophysiol. **27**(6), 626 (1969).
[48]E. Rojas and C. Hidalgo, Biochim. Biophys. Acta **163**(4), 550–556 (1968).
[49]D. Baetz, M. Bernard, C. Pinet, S. Tamareille, S. Chattou, H. El Banani, A. Coulombe, and D. Feuvray, Mol. Cell. Biochem. **242**(1–2), 115–120 (2003).
[50]M. Ten Hove, M. G. Nederhoff, and C. J. Van Echteld, Am. J. Physiol. - Heart Circ. Physiol. **288**(1), H287–H292 (2005).
[51]I. R. Efimov, V. V. Fedorov, B. Joung, and S. F. Lin, Circ. Res. **106**(2), 255–271 (2010).
[52]D. V. Abramochkin, V. S. Kuzmin, G. S. Sukhova, and L. V. Rosenshtraukh, Acta Physiol. **196**(4), 385–394 (2009).
[53]R. Furlan, S. Guzzetti, W. Crivellaro, S. Dassi, M. Tinelli, G. Baselli, S. Cerutti, F. Lombardi, M. Pagani, and A. Malliani, Circulation **81**(2), 537–547 (1990).
[54]T. M. Kolettis, Life Sci. **118**(2), 136–140 (2014).
[55]N. Hagiwara, H. Irisawa, and M. Kameyama, J. Physiol. **395**, 233–253 (1988).
[56]R. Wilders, H. J. Jongsma, and A. C. van Ginneken, Biophys. J. **60**(5), 1202–1216 (1991).
[57]S. Dokos, B. Celler, and N. Lovell, J. Theor. Biol. **181**(3), 245–272 (1996).
[58]J. Senges, T. Mizutani, D. Pelzer, J. Brachmann, U. Sonnhof, and W. Kubler, Circ. Res. **44**(6), 856–863 (1979).
[59]M. Kyriakidis, J. Barbetseas, A. Antonopoulos, C. Skouros, C. Tentolouris, and P. Toutouzas, Chest **101**(4), 944–947 (1992).
[60]T. Martins-Marques, S. Catarino, M. Zuzarte, C. Marques, P. Matafome, P. Pereira, and H. Girao, Biochem. J. **467**(2), 231–245 (2015).